Accurate Characterization of High-Q Microwave Resonances for Metrology Applications

IEEE Journal of Microwaves

Received 29 January 2021; revised 26 February 2021 and 27 February 2021; accepted 27 February 2021. Date of publication 29 March 2021; date of current version 7 April 2021.

Digital Object Identifier 10.1109/JMW.2021.3063247

Accurate Characterization of High-*Q* Microwave Resonances for Metrology Applications

CHIARA RAMELLA (Member, IEEE), MARCO PIROLA (Senior Member, IEEE), AND SIMONE CORBELLINI

(Invited Paper)

Department of Electronics and Telecommunications, Politecnico di Torino, 10129 Torino, Italy

CORRESPONDING AUTHOR: CHIARA RAMELLA (e-mail: chiara.ramella@polito.it).

This work was supported in part by EURAMET and the European Union under an EMPR Researcher Grant.

ABSTRACT Microwave resonators are widely adopted as high sensitivity sensors in both applied and fundamental metrology, to measure a number of different physical quantities, such as temperature, humidity, pressure, length and material properties. High sensitivity, and thus potential high measurement precision and accuracy, can be achieved by resorting to high-quality-factor (Q) resonators. Nonetheless, in order to accurately measure a high-Q resonance and obtain low measurement uncertainty, as required by metrology applications, the entire measurement set-up must be carefully designed. This papers presents an overview of resonance frequency measurements for metrology applications, illustrating the various aspects and issues to be dealt with when pursuing highly accurate measurements, as well as of the most relevant achievements in this field.

INDEX TERMS Cavity resonators, microwave metrology, microwave resonance, microwave sensors, whispering gallery resonators.

I. INTRODUCTION

Microwave resonators are key elements for the implementation of amplifiers, oscillators and filters. Beyond this, they have found widespread application as highly-sensitive sensors in industry (e.g., for moisture and displacement sensing applications [1]–[4]), scientific research and metrology [5]–[9]. In fact, among all physical quantities, frequency and time can be measured with exceptional accuracy, thus making microwave resonances one of the most interesting methods for measuring temperature [10], [11], pressure [8] and humidity [12], [13], for accurately characterizing permittivity, permeability, mass, density and water content for a variety of materials [9], [14] and for detecting foreign particles [15], since the resonance frequency of a microwave resonator depends on all these physical parameters. Moreover, high sensitivity, high speed, relatively low cost, high adaptability and flexibility and their non-destructive, non-contact nature are the main advantages of resonance-based measurements, together with their ability to take precise measurements within a small area.

The high sensitivity and thus the potential high precision and accuracy of resonance-based measurements is related to the quality factor (Q) of the resonator:

$$Q = \frac{f_{\mathrm{r}}}{BW} \tag{1}$$

where f_{r} is the resonance frequency and the bandwidth BW is defined as the full width at half maximum (FWHM, -3 dB). The higher Q, the higher the achievable resolution in determining the resonance frequency. Among others, quasi-spherical cavity resonators (QSRs) and whispering-gallery-mode dielectric resonators (WGMRs) demonstrated Q factors in the order of 10^4 to 10^6 and thus found application as primary metrology instruments [8], [10], [16]–[18] and transfer standards [19] as well as in fundamental metrological experiments for the determination of the Boltzmann constant [7], [20] and, nowadays, for the mise en pratique of the kelvin [21].

The resonance characteristics depend on the resonator's structure and geometry and are found by solving Maxwell's

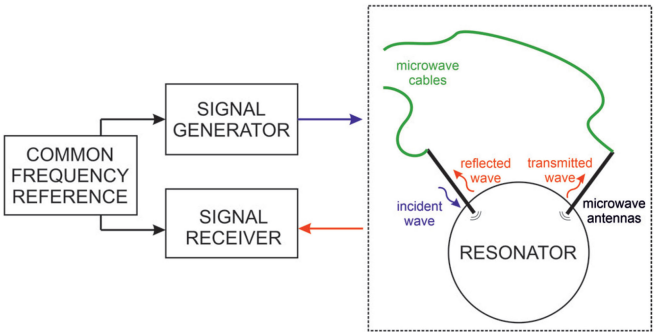

FIGURE 1. Measurement set-up for the identification of the complex resonant frequency of a microwave resonator. From this quantity, other physical parameters (of the resonator, of its content or of the environment) can be obtained as shown in Fig. 10.

equations with the resonator boundary conditions. This analysis leads to the *complex resonance frequency*

$$f_0 = f_r + jg_r \tag{2}$$

where the real part is the resonance frequency f_r itself and the imaginary part

$$g_r = \frac{f_r}{2Q} = \frac{BW}{2} = \Delta f \tag{3}$$

is the half-width of the resonance which represents the leaky term of the solution. For metrology applications high accuracy is fundamental, often at levels usually not necessary in common microwave applications, i.e. in the range of few parts-per-million (ppm) down to few parts-per-billion (ppb). The intrinsic high sensitivity and resolution of the resonator alone are not sufficient to guarantee high measurement accuracies, for which, as a matter of facts, the accuracy of the entire measurement set-up is a key factor. As depicted in Fig. 1 the resonator is coupled by means of a microwave antenna to a frequency swept signal generator that inject power into the resonator, exciting the desired resonant mode/modes. At resonance, more power is transferred to the resonator, thus, in principle, the resonance can be characterized either by measuring the power reflected by the resonator (or S_{11}) or the transmitted power (or S_{21}). The former exhibits a dip in magnitude at resonance, while the latter a peak in magnitude. In either cases a tuned signal receiver locked to the same frequency reference (time base) of the generator is adopted. However, as detailed later on, in practice transmission measurements are always preferred. In principle scalar transmission measurements should be sufficient to obtain both the real and imaginary parts of the complex resonance: the former is the frequency at which peak transmission occurs, while the latter is the span between the two −3 dB (half-power) frequency points. However, as shown in the following, in order to achieve a high level of accuracy with real resonators, parameter extraction from measurement fitting is practically mandatory.

This papers presents a brief overview of the current and potential exploitation of resonance frequency measurements in metrology, highlighting the critical and/or challenging aspects that such applications pose to the measurement setup, the instrumentation equipment and the data processing algorithms. The rest of the paper is organized as follows: Section II recalls the basics concepts of resonance modes; then, Sections III and IV discuss the various aspects of resonance measurements; finally, in Section V the main metrology applications of QSRs and WGMRs are presented.

II. RESONANCE THEORY REVIEW

A resonator is a "closed" structure that confines electromagnetic (EM) waves within it by means of reflection at boundaries and thus naturally resonates at specific frequencies. A cavity resonator is a metallic enclosure, either hollow or filled with some dielectric, thus it is the high conductivity of the metal walls that confines EM waves. A dielectric resonator is a solid object made of a high-dielectric-constant material, thus the reflection mechanism relies on an abrupt permittivity change at its surface. EM waves inside the cavity travel back and forth interfering each other, therefore, at frequencies where the resonator dimensions along a certain wave direction are multiple of half-wavelength, they create standing waves, leading to large oscillations, and store energy in the resonator. Whispering-gallery mode resonators, are peculiar dielectric structures in which confined standing waves are generated along the equatorial surface thanks to rotational symmetry along the central axis and total internal reflection mechanism.

Losses in cavity and dielectric resonators are due to, respectively, the finite conductivity of metallic walls and the dielectric losses. Cavity resonators are typically adopted at microwave frequencies, where the physical dimensions of the cavity can be reasonably small and metal losses are limited. Dielectric resonators are instead typically employed at higher frequency, where metal losses start to become non-negligible and higher than dielectric ones.

A resonator is typically a multi-mode structure, showing different resonant frequencies associated to different EM modes. Moreover, unless particular geometries are adopted to deliberately create a low-pass behavior, resonance occurs also at the harmonics of these fundamental frequencies, even if with weaker oscillation amplitudes.

The simplest resonators are shorted pieces of rectangular (prism resonator) or circular (cylindrical resonator) waveguides, either metallic or dielectric. Circular geometries are often preferred in practical applications, as they present lower machining cost and higher geometrical accuracy, which in turn gives higher Qs. Metallic waveguides, and thus cavity resonators, support only transverse electric (TE) and transverse magnetic (TM) modes, while in dielectric resonators hybrid electromagnetic modes (HEM) also exists due to imperfect boundary conditions, which are however low-Q modes and thus not of interest for metrology applications [22].

Resonant modes can be found mathematically by solving the wave equations inside the resonator considering the boundary conditions. For ideal resonators and simple geometries closed-form solutions are available, however for a very

accurate resonance model it is necessary to recur to numerical simulations, usually carried out by means of 3D finite-element (FEM) solvers.

A. CAVITY RESONATORS

Assuming perfectly conductive walls and homogeneous filling with a dielectric of permittivity ε and permeability μ, the resonance frequencies of rectangular, cylindrical and spherical resonators can be found analytically [23]. The homogeneous filling, together with the absence of internal sources, ensures that the divergence of the electric field is zero, while perfect conductive walls force zero tangential electric field at the metallic surface. The simple geometry allows the problem to be stated in terms of a scalar Helmholtz equation

$$(\nabla^2 + k^2)\psi_\zeta = 0 \tag{4}$$

where ∇^2 is the Laplacian operator, ψ_ζ is the scalar potential associated to the field vectors and k is the wave number. This is an eigenvalue equation, thus its non-zero solution is an infinite discrete set of eigenfunctions ψ_ζ associated to the eigenvalues k_ζ^2, where the index ζ is a multi-index given by a combination of the mode numbers ($\zeta = mnp$). The resonant frequencies (eigenfrequecies) are given by:

$$f_\zeta = \frac{k_\zeta}{2\pi\sqrt{\varepsilon\mu}} \tag{5}$$

Note that there may be degenerate modes having the same eigenfrequency for different combinations of the mode numbers.

1) SPHERICAL AND QUASI-SPHERICAL RESONATORS

Spherical resonators are the most interesting for metrology applications. Comparing the lowest-order modes of a spherical resonator of radius a with those of a cylindrical and a cubic resonator of roughly the same volume the former shows highest quality factor [23]. Moreover, the sphere shape can be manufactured with an higher degree of accuracy, confirming the possibility to achieve higher quality factor also when dealing with real resonators.

For a spherical cavity the Laplacian can be expressed in (r, θ, ϕ) coordinates and the Helmholtz equation in (4) is obtained by defining TE and TM modes with respect to r, i.e. considering concentric spherical waves. The field solution can be written in terms of sinusoids, Legendre functions and spherical Bessel functions (and their derivatives). The relationship between the resonance frequencies and the cavity radius a is

$$f_{mnp}^{\mathrm{TE}} = \frac{u_{np}}{2\pi a\sqrt{\varepsilon\mu}} \tag{6a}$$

$$f_{mnp}^{\mathrm{TM}} = \frac{u'_{np}}{2\pi a\sqrt{\varepsilon\mu}} \tag{6b}$$

for TE and TM modes, respectively, where u_{np} and u'_{np} are the p-th zeros of the n-th order spherical Bessel function and of its derivative, respectively. Since resonance frequencies are independent of m, many degenerate modes, at least triplets, are present in a spherical cavity.

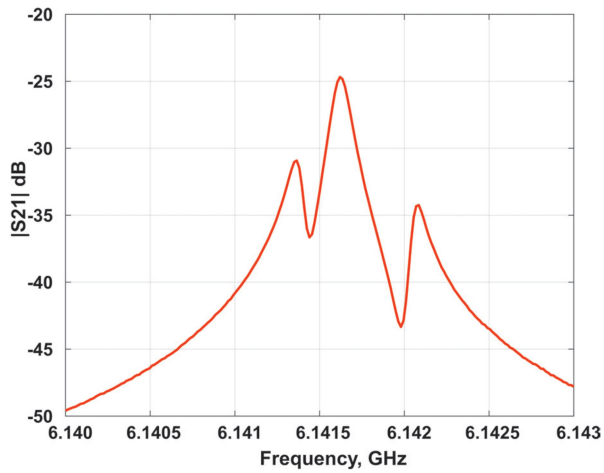

FIGURE 2. Transmission profile of a QSR triplet: peak separation can be visually appreciated even though the separation between the farthest peaks is within 120 ppm. The three individual resonances can be found with fitting as reported in Fig. 9.

The higher Qs, together with excellent acoustic properties of spherical resonators (non-degenerate, radially symmetric and very high Q acoustic resonant modes together with insensitivity to viscous damping at the boundaries [24]) made them a preferable choice for metrology applications. However, only in an ideal sphere the three peaks are perfectly superimposed. In real resonators, instead, they are not coincident but at the same time too close to be distinguished, hence the overall effect is a single peak with larger bandwidth. To overcome this issue, quasi-spherical resonators (QSRs) have been developed [16]. In a QSR, degenerate modes separation is intentionally amplified, as shown in Fig. 2, by transforming the sphere into a triaxial ellipsoid with axes a, $a + \delta a_1$ and $a + \delta a_2$. As analytically shown in [25]–[27], the fractional splitting is determined by the two parameters $\delta a_1, \delta a_2 \ll 1$. The mean resonance frequency is still given by (6) substituting the radius a with the equivalent radius a_{eq} as demonstrated in [28].

2) MICROWAVE CAVITY PERTURBATION

In many cases cavity-resonator-based measurements rely on the microwave cavity perturbation (MCP) approach [8], [29]. Any variation in the dielectric characteristics of the material that fills the cavity is translated into a variation of the resonance frequency and, if the material is lossy, of the resonance bandwidth (i.e. complex frequency shift). By taking two subsequent measurements, a first with the empty (*unloaded*), cavity and a second after introducing the sample that is object of the measurement into the resonator (*loaded* cavity) the dielectric or physical properties of the sample can be obtained. The sample can completely fill the cavity, as in gas characterization [13], or only a portion of its volume.

Under the assumption of small perturbation, i.e. when perturbed and unperturbed fields are approximately the same, the

relationship between the change in the complex permittivity and/or permeability of the sample and the complex resonance frequency can be written as [30], [31]

$$\frac{\delta f_0}{f_0} = \frac{\delta f_r}{f_0} + j\frac{\delta g_r}{f_0} \approx -\frac{\int \delta\varepsilon|\overline{E}|^2 + \delta\mu|\overline{H}|^2 dV}{\int \varepsilon|\overline{E}|^2 + \mu|\overline{H}|^2 dV} \quad (7)$$

where $\overline{E}$ and $\overline{H}$ are the unperturbed electric and magnetic fields and dV denotes integration on the associated volume. The MCP assumption holds for small $\delta\varepsilon$ and/or $\delta\mu$ or when the sample has a small volume compared to the cavity and it is properly placed inside it (at a standing wave maximum and parallel to the field of interest). With the MCP approach, the quantity of interest is not the absolute complex frequency but its drift, obtained from the ratio between the loaded (f_0') and unloaded (f_0) resonance frequency:

$$\frac{\delta f_0}{f_0} = \frac{f_0'}{f_0} - 1 \quad (8)$$

B. DIELECTRIC RESONATORS

Dielectric resonators gained interest in microwave oscillators, filters and antennas design thanks to their reduced dimensions with respect to waveguide based components. In fact, for the same resonance frequency, the size of a dielectric resonator made out of a high-permittivity material is sensibly smaller than that of an empty cavity, hence lowering weight and cost and easing ingratiation, while it shows comparable temperature stability. Moreover, at increasing frequency, metal losses becomes non-negligible and dielectric resonators outperform cavity ones also in terms of Q [32]. Beyond this, dielectric resonances are used to characterize the complex permittivity and permeability of dielectric materials [33]–[35].

In a dielectric resonator, the open circuit boundary conditions are only approximately satisfied, thus EM fields components extend outside the resonator. Due to these non-idealities, (4) becomes transcendental and must be thus solved numerically or with approximated approaches, even for simple geometries. Dielectric resonators of practical interest are cylindrical resonators in which the strongest mode is the $TE_{01\delta}$ mode. An approximated formula for its resonance frequency is given in [32] for an isolated cylindrical resonator. In any case, dielectric resonators are practically never used as isolated object, but they are either coupled to microstrips (e.g. in antennas) or enclosed in a metallic shielding cavity. The resonance frequencies of the cavity and those of the dielectric resonator interfere each other, and hence must be computed considering the coupled structure [36].

1) WHISPERING GALLERY MODE RESONATORS

A particular class of microwave resonances occurring in dielectric resonators is represented by whispering gallery modes (WGM) [37]. In uniaxial anisotropic dielectric resonators with round edges (spheres or cylinders, but also disks or rings) 2D EM waves are bounced around the resonator's equatorial circumference due to almost-total internal reflection at the surface (i.e. with negligible reflection losses). Constructive interference arises if after an entire roundtrip a wave comes back in the same point with the same phase, thus creating a standing wave. Such standing waves are characterized by large electromagnetic fields confined very close to the dielectric surface and extremely high quality factors.

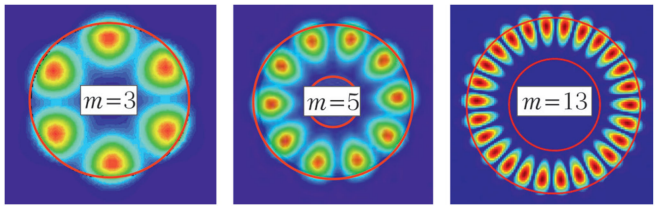

FIGURE 3. 2D field map of whispering gallery modes ($n = 1$).

Under the assumption of a 2D dielectric circle of radius a, the problem can be again stated in terms of a scalar Helmholtz equation of the form of (4). The boundary conditions are that the eigenfunctions should be finite everywhere, be continuous at the edge of the cavity and describe only outgoing waves, and can be satisfied by a combination of sinusoids, Bessel and Hankel functions. The characteristic equation is transcendental and thus can only be solved numerically, obtaining the complex eigenfrequencies f_{mn}. The index m is the order of both the Bessel and Hankel functions and it is related to how many times the wave is reflected in one round-trip. The higher m the more the energy is confined close to the surface as shown in Fig. 3. The index n, instead, indicates how many times the mode can oscillate inside the resonator (toward the center), thus modes that are of practical interest are only those with $n = 1$, since for higher n values energy is not well localized near the boundaries. Thanks to this field localization and to the total reflection mechanism, which better confines modes inside the resonator, WGMs have higher Qs with respect to most of the other dielectric modes, in excess of 10^5 at microwave frequencies and up to 10^9 for optical modes [38]. Optical WGMRs are thus widely adopted to implement photonic integrated circuits (filters, generators, storage devices), and ultra-low-threshold/single-atom microlaser, in interferometry, spectroscopy, quantum electrodynamics and fluorescence studies, as well as for metrology and sensing applications, in particular biosensors [39]. Nevertheless, microwave and millimetre-wave WGMRs, made of low-loss single crystalline materials (quartz, sapphire, ruby, ect.), do also show remarkable quality factors finding applications both in high-performance microwave components and as high sensitivity sensors for thermometry [11], spectroscopy [40] and accurate complex permittivity measurements [41].

Independently of the frequency range, the operating principle of a WGMR sensors relies on the fact that, due to the evanescent field outside the cavity, any variation in the surrounding environment (temperature, pressure, chemical composition, etc.) is translated into a resonance frequency shift and/or change in the resonance bandwidth, i.e. in a variation of the complex resonance frequency. The measurement, in this case is usually not differential, as in MCP-based sensors, but

absolute and consists in monitoring the WGM resonance in time and gathering the desired physical quantity by knowing its relationship with the observed resonance value. Thanks to the large Qs of WGMs, even small shifts can be appreciated and thus a high sensitivity is reached. WGMRs are particularly sensitive to temperature, due to both thermal expansion and permittivity (and hence refractive index) dependence on temperature. Considering the ideal case of a 2D disk, we can write

$$\frac{\partial f_r}{\partial T} = \frac{\partial f_r}{\partial \varepsilon_\perp}\frac{\partial \varepsilon_\perp}{\partial T} + \frac{\partial f_r}{\partial \varepsilon_\parallel}\frac{\partial \varepsilon_\parallel}{\partial T} + \frac{\partial f_r}{\partial a}\frac{\partial a}{\partial T} \tag{9}$$

where $\varepsilon_\perp$ and $\varepsilon_\parallel$ are the dielectric permittivities in the radial and axial direction, respectively, while a is the radius of the disk, which undergoes thermal expansion. Also in case of 3D structures the thermal expansion along the axial direction is negligible with respect to that along the radial one, and (9) is still approximately valid. Moreover, with the typically adopted dielectrics, the thermal expansion is roughly one order of magnitude lower than the permittivity change in temperature, thus its impact on the resonance shift is small. Temperature sensitivity is at the base of WGM thermometry (WGMT), but represents an issue in all other sensor applications. For this reason, in many cases, multi-modal sensing is used. This technique is based on measuring the frequency splitting between two coupled modes rather than the resonance frequency of a single one, so that thermal shifts become a common-mode phenomenon (modes have the same thermal sensitivity).

An ideal WGMR features perfect rotational symmetry along a central axis. If this symmetry is perturbed in any way, the mode splitting phenomenon arises [42]. Due to the asymmetry, the two counter-propagating standing waves accumulate sightly different phase shift along each revolution, thus creating two separated resonance frequencies as shown in Fig. 4. For resonances in the order of 10 GHz, depending on the level of asymmetry, the split can easily go from below 1 MHz for quasi-ideal WGMRs, corresponding to less than 100 ppm, up to more than 10 MHz. In principle, mode splitting can be intentionally forced to avoid degeneracy as in QSRs, provided that the introduced asymmetry is controlled. In [43] this phenomenon was exploited to assess possible mechanical instabilities of the developed WGMT.

III. RESONANCE MEASUREMENT SET-UP

Microwave resonances are typically extracted from S-parameter measurements. The basic set-up depicted in Fig. 1 is still valid, with the only difference that the measured quantities are not the absolute waves but power ratios between the reflected or transmitted wave and the incident one. S-parameter measurements are typically carried out by means of a vector network analyzer (VNA), which contains both the signal generator and the receiver. A 2-port VNA automatically performs a frequency sweep at the input port and measures, at each frequency step, the incident and reflected waves at both ports, computing the 4 S-parameters of the network under test [44].

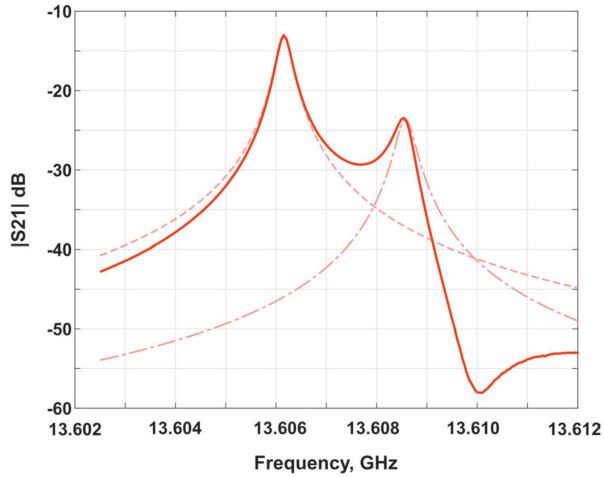

FIGURE 4. Transmission profile of a WGM with forced mode splitting: the overall spectrum (solid) is given by the superposition of two separate modes (dash, dot-dash obtained with fitting) with relative separation in the order of 200 ppm.

Reflection-based measurements would have the advantage of requiring just a single antenna and one-port analysis. However, the reflection dip tends to be very small, while, on the contrary, the background reflection (out of resonance value of $|S_{11}|$) tends to be almost unitary, since antennas are intentionally weakly coupled to avoid overloading the cavity (see Section III-A). Moreover, reflection measurements are much more sensitive to the effect of the connecting cables and would thus require a more accurate calibration of the measurement system. Despite requiring a second antenna and a 2-port analysis, transmission measurements are much more reliable and accurate. In fact. $|S_{21}|$ typically exhibits large peak magnitudes with respect to background transmission.

From an electrical point of view, the system of Fig. 1 can be represented by the equivalent circuit of Fig. 5: the signal generator is a sinusoidal source voltage V_S with source impedance Z_S, while the receiver is modeled as a load impedance Z_L. With standard instrumentation $Z_S = Z_L = 50\,\Omega$. The resonator, or better, the resonant mode of interest, is modeled with a series RLC circuit.

$$Z_R = R + j2\pi fL - j\frac{1}{2\pi fC} = R\left[1 + jQ\left(\frac{f}{f_r} - \frac{f_r}{f}\right)\right] \approx R\left[1 + j2Q\left(\frac{f - f_r}{f_r}\right)\right] \tag{10}$$

where the quality factor Q and resonance frequency f_r are

$$Q = \frac{1}{R}\sqrt{\frac{L}{C}} \quad \text{and} \quad f_r = \frac{1}{\sqrt{LC}} \tag{11}$$

Microwaves are coupled to electromagnetic fields inside the resonator by means of coaxial antennas. Open-circuit probe antennas and short-circuited loop antennas are the most

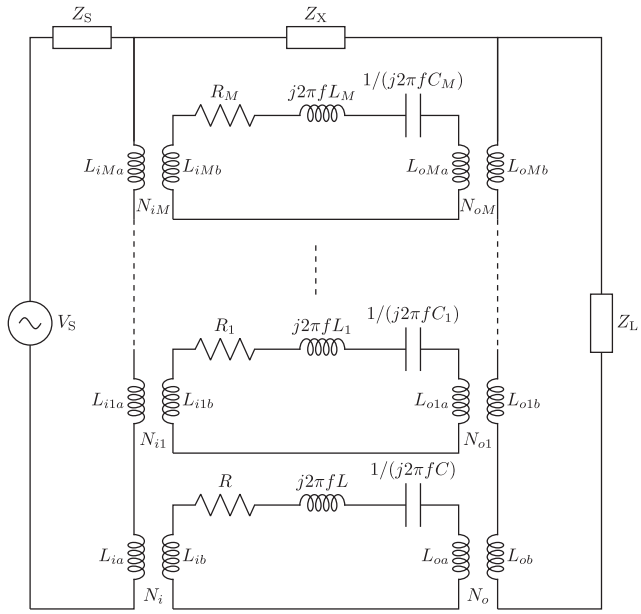

FIGURE 5. Simplified circuit model of a resonance measurement set-up.

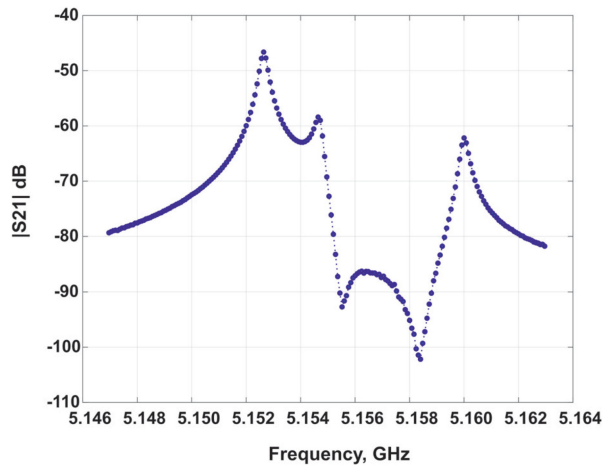

FIGURE 6. Example of a measured QSR $|S_{21}|$: due to the extremely weak coupling the three resonance peaks are all below −45 dB, with the lowest one below −60 dB, while transmission background is below −80 dB.

widely adopted solution for coupling with the electric field along the cable axis or with the magnetic field perpendicular to the loop area, respectively. Complete theories for the excitation of modes in a cavity can be found in [45] and [46]. An antenna can be modeled with an impedance transforming network where the equivalent turns ratio N is representative of the coupling strength. For loop antennas a finite self inductance L can be also included. Impedances Z_X and the M RLC circuits in parallel are added to model crosstalk and unwanted/spurious modes, respectively, as detailed in the following.

A. RESONATOR AND ANTENNA DESIGN

The microwave resonator is designed resorting to FEM simulations. It should be sized so as to have high Q resonant modes at suitable frequencies, as well as to be practical for the experiment of interest. Manufacturing cost and tolerances, mechanical stability, cavity sealing, weight and ease of integration of antennas and/or other connecting or support elements are a not exhaustive list of all the practical aspects that must be considered in selecting the most appropriate geometry, size and assembly of the resonator. Material choice is a key factor for achieving high performance. For metallic cavities, a highly conductive material must be selected. Silver and copper show highest bulk conductivities, however they are subject to aging and oxidation, which would have a detrimental impact on the effective surface conductivity. Gold plated copper is thus the usual choice, which ensures a sub-optimum but fairly good and stable conductivity. Concerning WGMRs, quartz is the most commonly adopted material for optical applications. At microwave frequency, even if ruby has been also considered in some experiments [47], synthetic sapphire is the material of choice thanks to extremely low losses over a wide operating temperature range [48].

Antenna design and positioning is one of the most critical points to obtain accurate measurements. Several aspects must be considered:

1) OVERCOUPLING: "unloaded" cavity resonances in a strict sense exist only in a mathematical world. In practice, all the measured cavity resonances are "loaded" by the presence of the antennas, and thus show loaded quality factors always lower than the theoretical ones. To achieve high sensitivity it is thus fundamental to keep cavity loading as low as possible. This can be practically accomplished with a sort of "try and error" minimization approach. The antennas are first pushed relatively deeply inside the resonator and the obtained loaded Q is measured. Then the antennas are extracted in small steps until improvements are observed in the obtained Qs. This usually leads to very low transmission peaks, as shown for example in Fig. 6, which represent a challenge for the receiver in terms of dynamic range. As a final remark, note that injecting large powers into the cavity would possibly lead to heating due to microwave losses. Even if this effect is typically negligible, it can become an issue when working at cryogenic temperatures [49].
2) CROSSTALK: microwave antennas are radiating objects, thus some direct power transfer between them may take place. Such crosstalk effect represent a non-zero background transmission and it is modeled in Fig. 5 with an impedance $Z_X(f)$ directly connected between the input and output ports. Outside the cavity, other possible sources of direct power leakage between the transmitter and the receiver may be due to electro-magnetic coupling along the cables or low port isolation within the VNA.
3) MULTI-MODE EXCITATION: a resonator is inherently a multi-mode structure, hence a number of modes

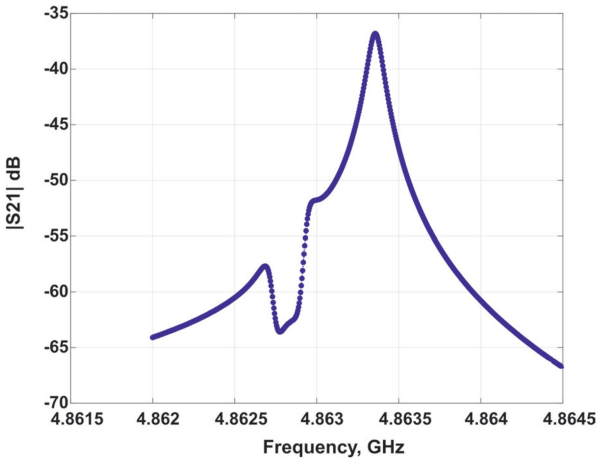

FIGURE 7. Example of a measured QSR $|S_{21}|$: due to antenna positioning, only one peak is visible while a transmission drop appears due to the interference of the other two as confirmed by the fitting reported in Fig. 8(a).

different from the desired one(s) are inevitably excited by the antennas. All these modes have transmission tails that fall in the measurement bandwidth and that interfere each other and with the mode(s) under test. The observable effect is a non-constant transmission background possibly showing transmission minima at some frequency interfering with the peaks, as shown for example in Fig. 6. Moreover, when more than one mode is under investigation, as in QSRs, reciprocal interference of these mode can have similar destructive effects, as shown for example in Fig. 7. Here the transmission background is clearly much lower than the resonance, however, the phase relationship within the modes in the triplet causes two of the three peaks to virtually cancel each other out. In both cases it is clear that manually finding the transmission maxima is not possible, hence requiring resonance fitting. Mode interference is determined by the position of the two antennas, thus moving them can alleviate or exasperate this phenomenon. Although optimum positioning can be pursued before taking the measurement, both the resonance shape modification and the complicated background that result from mode coupling, as well as crosstalk can, and should, be accounted for by the fitting procedure, allowing for accurate identification also in the presence of such non-idealities. Each mode can be represented by an equivalent RLC circuit in parallel with the main resonance [50] and coupled to the antennas with its own coupling factor, as shown in Fig. 5.

4) MODE ALTERATION: the presence of the antennas requires having through holes in the cavity surface, presenting a localized reactive impedance. This, in turn, alters the standing wave patterns of all the excited modes, with the practical effect of loading the cavity and reducing the quality factor and increasing the attainable measurement uncertainty. Antennas should thus be fabricated out of high conductivity materials, keeping their electrical size and impedance as small as possible to maintain high Qs. The loading effect of antenna holes in QSRs was investigated in [51] by treating them as waveguides. By applying proper correction factors on the fitted resonances its impact can be limited, but not eliminated.

B. SIGNAL GENERATION AND ACQUISITION

The characterization of high-Q microwave resonances by direct measurement of f_r and g_r would require very high frequency resolution to reach ppb-level accuracy. However, as detailed in Section IV, resonance fitting is always applied that relaxes the resolution requirement by several order of magnitudes.

The signal receiver must comply with two main requirements: vector measurement capability and high dynamic range. Typical peak values of $|S_{21}|$ at resonance are in fact 10 dB to 60 dB above transmission background [43]. Thus, accounting for resonance amplitude variability, a minimum dynamic range of 60 dB is required. Signal acquisition in modern VNAs is performed with a superheterodyne receiver that down-converts the transmitted signal to an intermediate frequency (IF) suitable for direct analog-to-digital conversion. This approach allows for harmonic rejection and dynamic range improvement thanks to the use of highly selective IF filters (with bandwidths as low as 10 Hz or even 1 Hz in high-end VNAs) and, eventually, IF amplifiers and digital filters. The latter reduce the noise floor by eliminating out-of-band spectral components, while the former amplify the useful signal both contributing in enhancing the measurement signal-to-noise ratio (SNR).

VNAs are typically expensive and bulky instruments, thus may represent a main bottleneck to the application of resonance-based measurements to industrial metrology. As demonstrated in [52] and [53], for such application the capabilities of a VNA are redundant and a portable and low-cost system can be developed ad-hoc tailored to resonance measurement, based on these considerations:

1) MEASUREMENT TYPE: only the transmission parameter S_{21} is required, thus the computation of all other parameters can be avoided.
2) MEASUREMENT SCALABILITY: object of the measurement are not the absolute values of the transmission magnitude and phase but the complex resonance frequency (position of the peak and half-power bandwidth), thus S_{21} can be scaled to any arbitrary complex normalization constant K (i.e. KS_{21} can be measured instead of S_{21}).
3) MEASUREMENT BANDWIDTH: only few modes are of interest for a specific application, whose approximate resonance frequencies are known a priori from theory and/or simulations. Therefore, an ad-hoc system covering only a limited frequency range can be developed, avoiding using multiple oscillators as in broadband VNAs.

4) CALIBRATION: high-Q modes require measurements over a very narrow frequency span (2 MHz to 10 MHz). This, in practice, makes calibration desirable but not mandatory, thanks to the capability of the fitting function to properly model narrow-band transmission backgrounds (more details are given in Section IV).

On the other hand, vector measurement capability of the VNA must be retained. Since the imaginary part of the complex frequency is given by the bandwidth, scalar (magnitude) S_{21} measurement should be in principle enough, which can be also obtained with a power meter or a spectrum analyzer. However, fitting algorithms in the complex frequency domain require less input points to converge, are faster and, above all, they are more robust and provide lower fitting uncertainty (for the same number of points). Moreover, they can better model the background transmission, particularly important in absence of calibration.

1) FREQUENCY REFERENCE

To perform a frequency measurement, a frequency reference is required, i.e. a stable oscillator that generates an accurate fundamental frequency to synchronize the generator's and receiver's time-bases. This can be either a crystal oscillator (XO) or an atomic frequency standard (rubidium, cesium, or hydrogen), depending on the required accuracy. Commercial VNAs offer the possibility to be locked either to an internal 10 MHz reference, typically a quartz oscillator, or to an external frequency reference, in order to allow for synchronization among different instrument and/or frequency accuracy improvement.

The relative accuracy of the frequency reference is reported one-to-one to the measured frequency therefore for applications where the absolute resonance frequency must be known with a predefined (high) accuracy a high accuracy frequency reference is mandatory. In case of MCP-based measurements, the accuracy requirement can be relaxed provided that short-term stability is good enough to consider both measurements (unloaded and loaded cavity) affected by approximately the same frequency error. Short-term stability is indeed rather good, in the order of some parts per trillion (ppts), for all cited frequency reference types, as reported in [54]. Long-term stability, instead, ranges from 0.1 ppb/day and 1 ppm/year for standard XOs to less than 0.1 ppt/day and 0.1 ppb/year for atomic standards. Similarly, temperature drifts go from 0.1 ppm/K in XOs, to 0.1 ppb/K in oven controlled crystal oscillators (OCXOs) and down to few ppt/K for cesium standards. From these number it is possible to conclude that for MCP-based applications dedicated instrumentation is typically not required, since the internal VNA reference is sufficient. High-end VNAs reach in fact frequency reference accuracy between 1 ppm and 50 ppb, stability between 1 ppm/year and 0.1 ppm/year and drift between 1 ppm/K and 10 ppb/K. On the other hand, these values are clearly not compatible with demanding applications, such as WGMT or refractive index gas thermometry (RIGT), where an absolute frequency must be characterized with high accuracy. For such experiments external frequency standards are adopted. Rubidium standards are preferred, when possible, since they are cheaper and more compact than cesium ones. They can provide accuracies in the order of 50 ppt, which is enough for most resonance measurements applications, but their performance can be further enhanced if disciplined by a GPS/GNSS receiver, reaching accuracies comparable to cesium standards, i.e. in the order of fractions of ppt. Again, frequency reference are typically expensive and bulky, thus in [53] a compact and low-cost alternative has been developed, based on the concept of GPS disciplined oscillator (GPSDO), but applied to a low-cost OCXO rather than to a high-end standard, achieving accuracy and stability within 1 ppb.

IV. RESONANCE FITTING

The acquired S_{21} data are sent to a processing unit to gather the complex resonance frequency and consequently the physical quantity of interest (permittivity, temperature, pressure, etc.). As anticipated, the real and imaginary parts of the complex resonance frequency may in principle be simply obtained by inspecting $|S_{21}|$ (scalar measurement), finding the peak (f_r) and the -3 dB frequency (g_r) points. However, this approach has two main drawbacks that make it incompatible with applications requiring high accuracy:

1) RESOLUTION AND MEASUREMENT SPEED: it would require a frequency resolution at least equal to the target accuracy, which means up to the ppb-level for metrology applications requiring absolute resonance frequency measurement. Furthermore, in practice, measured signal is always affected by noise. This directly limits the accuracy in the identification of the peak, thus hampering the advantages of having an high Q and requiring a frequency resolution even higher than the target accuracy. Even if achieving high resolution in modern signal generators may be not a big deal, working with such a high number of frequency points sensibly increases measurement time, which impacts on the required short-term stability of the entire set-up and may hinder the possibility to observe fast fluctuations of the quantity of interest.
2) BACKGROUND: in multi-mode resonators, i.e. in almost any practical case, the resonance frequency is affected by transmission background and mode interference. In worst cases, like that depicted in Fig. 7, the peak and -3 dB points cannot be directly measured at all (see also Fig. 8(a)). But in many cases, as for example that in Fig. 2 the measured points differ to some extent from the actual f_r and g_r values, as confirmed by resonance fitting reported in Fig. 9. This can be acceptable only when low accuracy is enough, but it is not the case of metrology applications, where accuracies better than 100 ppb are required.

To overcome these issues and achieve accurate frequency measurement, a relatively small number of frequency points are acquired over a bandwidth that is much larger than the

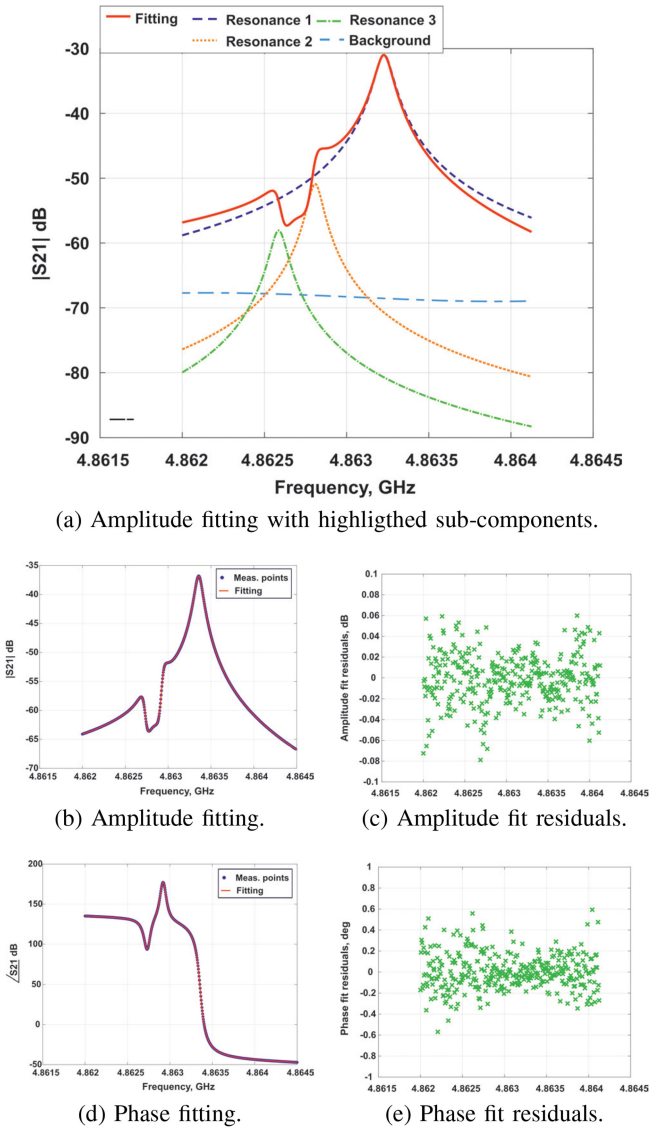

(a) Amplitude fitting with highligthed sub-components.

(b) Amplitude fitting.

(c) Amplitude fit residuals.

(d) Phase fitting.

(e) Phase fit residuals.

FIGURE 8. Detailed fitting results of the triplet in Fig. 7.

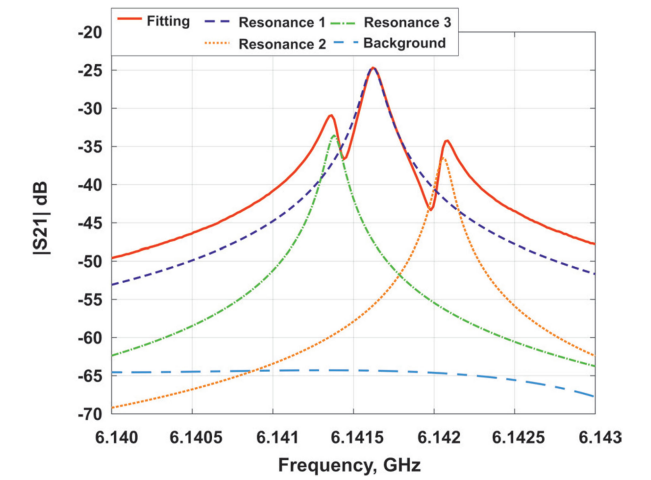

FIGURE 9. Detailed amplitude fitting results of the triplet in Fig. 2.

−3 dB one of a single peak and then fitted to a proper mathematical model. As a rule of thumb, 200 to 400 points are a good compromise between fitting accuracy and measurement speed. The measurement bandwidth should be well representative of the mode or modes of interest, including a large portion of the tails to properly fit also the transmission background. Proper choice of the bandwidth is fundamental but strongly depends on the resonator conditions within a particular experiment. For example, compare the situation of Figs. 6 and 2: in the first case the three peaks are much more separated (more than 2 MHz), which could depend on cavity sealing, and thus the measurement bandwidth is more than 15 MHz, which means 0.3% relative bandwidth and minimum frequency step of 75 kHz (15 ppm). In the second case the whole triplet and tails are within 3 MHz that means instead 0.05% relative bandwidth and 15 kHz minimum resolution, corresponding to roughly 2 ppm.

Note that, even for less accuracy-demanding applications, curve fitting is always a preferable approach as it allows to minimize the number of frequency points to be acquired, and thus speeds up the measurement procedure.

A. MATHEMATICAL MODEL

One of the first resonance models was introduced in [55] for acoustic resonances, based on complex Lorentzian functions. In [56] it was then demonstrated that such a model applies also to microwave resonances. A transmission peak is modeled with the following function:

$$S_{21} = \frac{\alpha f}{f^2 - f_0^2} \tag{12}$$

where α and f_0 are the complex parameters to be fitted, the latter being the complex resonance frequency of interest. The frequency term at the numerator allows for modeling of asymmetrical (skewed) resonances. In case of n degenerate modes, the superposition principle can be used, thus fitting each mode with (12) and summing them up. In a real resonator, non-zero background transmission is always present due to cross-talk, to the tails of neighbor resonance modes and to the effect of cables and connectors in case of uncalibrated or partially-calibrated measurements. All these contributions are modeled with a polynomial background function of the form that adds up to the Lorentzian(s). Thus the final resonance model of a n-tuple resonance is:

$$S_{21} = \sum_{i=1}^{n} \frac{\alpha_i f}{f^2 - f_{0,i}^2} + \sum_{j=1}^{p} \beta_j (f - f_c)^j \tag{13}$$

where f_c is the center frequency of the measured range, and β_j are additional complex parameters to be fit besides a_i and $f_{0,i} = f_{r,i} + jg_{r,i}$. Parameters are fitted through a Lavenberg-Marquardt algorithm. As suggested in [55] the minimization algorithm works separately on the sum of the squared residuals for the real and imaginary parts of (13).

The order p of the polynomial depends on the width of the measured frequency range and the amount of cross-talk. A

TABLE 1 Microwave-Related Uncertainty Contributions in the Determination of the Resonator Size in the Boltzmann Experiment of [57]

Source of uncertainty	Uncertainty contribution
Resonance fitting (repeatability)	16 ppb
Surface conductivity (skin depth)	40 ppb
Waveguide correction	116 ppb
Dielectric layer	113 ppb

quadratic background proved to be sufficient in MCP-based measurements with a calibrated VNA [13], while a 4-th order background was necessary to account for the higher required accuracy and relatively poor isolation of the adopted low-cost instrument in the WGMT experiment in [11]. In the RIGT experiment of [18], instead, a polynomial order as high as 7 was selected to account for background variations over the measured temperature range. Depending on the specific experiment, additional corrections such as shape and waveguide corrections reported in [18] and [51] for QSRs, can be subsequently applied to the fitted values to further improve the measurement.

To highlight the capabilities of the fitting algorithm to recover background and mode mixing effects, Fig. 8(a) details the results of the fitting of the "bad" triplet of Fig. 7. As can be noted, in this case two of the three Lorentzian resonances are very low compared to the other, which represent a worst-case situation for the fitting algorithm. Nevertheless, the overall resonance profile was well fitted both in magnitude and phase as shown in Fig. 8(b) to 8(e). Remarkably, deviations between the measured and fitted points are within 0.08 dB and 0.6°. In Fig. 9, the same results of Fig. 8(a) are reported for the "good" resonance triplet of Fig. 2. Note that, even if destructive interference among degenerate modes is not present, the actual (fitted) resonance frequency of the two side resonances does not coincide with their peak frequency, but differs form the latter by nearly 2.5 ppm. This confirms the need of resonance fitting to achieve sub-ppm accuracy.

Despite the high sensitivity of a resonator and the very low fitting uncertainties that can be achieved, in many practical cases the final measurement uncertainty is limited by the set-up non-idealities, such as imperfect cavity polishing or condensation and the presence of the antenna holes. As an example, Table 1 reports the microwave-related terms of the uncertainty budget in the determination of the resonator size in the Boltzmann experiment of [57]. As can be noted, the uncertainty related to the fitting algorithm is the lowest, while the residual error of the waveguide correction [51] and the effect of an unwanted dielectric layer on the surface lead the highest contributions (10 times higher than fitting repeatability).

B. BENCH CALIBRATION AND FITTING ISSUES

In many practical cases, VNA calibration up to the actual resonator's reference planes results impossible, since coaxial antennas are typically brazed to the resonator to ensure better coupling and mechanical stability/repeatability. Moreover in MCP-based experiments that require opening the resonator to insert a physical object, this procedure typically vanishes the validity of calibration, at least close to the cavity. Fortunately, the background term in the fitting function (13) is capable of recovering cross-talk effects due to test bench, even with uncalibrated measurements. The use of calibration, when possible and up to reference planes as close as possible to the resonator, is however preferable, in order to relax the order of the background polynomial, thus reducing the number of parameters to be fitted.

It is to note, in fact, that even with large polynomial order, the background function hardly copes with phase rotations over the measurement range, especially in case of relatively high background levels, as it is not able to fit both large magnitudes and wide phase variation at the same time. Large phase rotation is the typical effect introduced by microwave cables whose length is not negligible in the bandwidth of interest, as was the case of the experiment reported in [58], where the coaxial cable welded to the cavity were roughly 1 m long. A possible solution could be time-domain reflectometry, to measure the electrical length of the cables and correct the measurements accordingly. However, an effective but far simpler method was proposed in [58] that is to numerically correct the raw measurements with a phase rotation term found with minimization of the sum of squares of fit residuals over the entire frequency range, a function accomplished by the fitting algorithm itself.

V. RESONANCE BASED METROLOGY

One of the first use of a microwave resonator in a fundamental metrology experiment is reported in [5] and dates back to the late '40s. In this case, a cylindrical cavity was adopted to determine the speed of light in vacuum with an uncertainty of 30 ppm. Since then, microwave resonators kept attracting the metrology community, becoming the reference method for accurately measure the complex permittivity of dielectric materials and standards [59] as well as for the characterization of pure gases and mixtures, with potential application to hygrometers and humidity standards [9], [12] and to pressure standards [8].

After the institution of the International Temperature Scale of 1990 (ITS-90), quasi spherical resonators gained a major role in primary thermometry [10], [18], [60], allowing for discovering discrepancies between ITS-90 and thermodynamic temperatures. QSR-based experiments also played a crucial role in the determination of the Boltzmann constant [7], [20], [57] and are now considered paramount for the direct dissemination of the kelvin [21]. More recently, sapphire whispering gallery thermometry has been also proposed with potential application as industrial transfer standard [19], [48] but potentially also as interpolating thermometer [11].

Modern metrology applications demand for accuracies in the determination of the resonance frequency in the order of few parts per billions. At present, the main limitation is represented by bench non-idealities, as shown in Table I. On

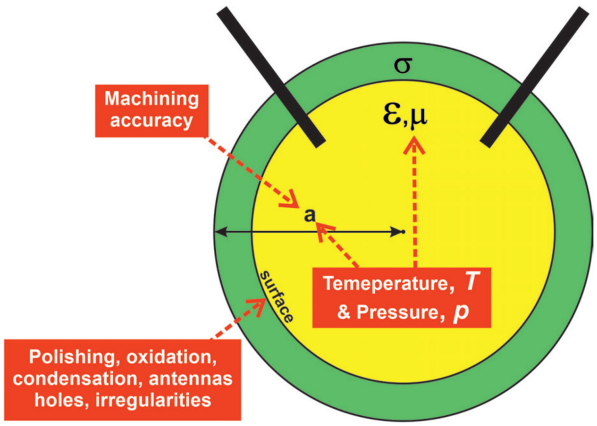

FIGURE 10. Dependence of the complex resonance frequency of a resonator to physical parameters.

the other hand, for the development of practical thermometers for the dissemination of the kelvin, field portability and cost of resonance-based thermometers must be enhanced, for which it is necessary to resort to custom-developed instrumentation.

A. QSR METROLOGICAL APPLICATIONS

The interest for spherical resonators aroused long ago, since the end of the '70s, when their potentialities in providing accurate measurements of resonance frequencies were first exploited for acoustic applications. In [24], [61] acoustic resonances of radial modes within spherical resonators were exploited to accurately measure the speed of sound in gases, contributing to the development of the so called primary acoustic gas thermometry (AGT). In the same papers, the combined use of acoustic and microwave resonance measurements was proposed.

Since the middle '80s, the QSR became a key element in the majority of those metrological experiments where measurements of length, pressure, dielectric properties and temperature, have to be related each other with exceptional accuracy, as in the case of primary thermometry. As shown in Fig. 10, all these elements are physically related to each other and to the complex resonance frequency.

As an example, QSRs along with cylindrical resonators played a fundamental role in the redefinition of the Boltzmann constant (k_B) that was one of the key requirements toward the definition of the new SI, based on the redefinition of four base SI units (kilogram, ampere, mole and kelvin), which took place in May 2019 and that is now considered a milestone in the history of the global metrology. Despite many primary thermometry methods have been used for the re-determination of the Boltzmann constant, AGT has emerged as the most important one, also by virtue of the simple relationship between the thermodynamic temperature T and the average kinetic energy of a molecule and therefore to the speed of sound w_0:

$$k_B = \frac{w_0\, M}{T \gamma_0 N_A} \tag{14}$$

where M represents the average molar mass of the gas, N_A the Avogadro constant, γ_0 the heat capacity ratio, which is exactly 5/3 for a monoatomic gas. Even if this experiment seems to be purely acoustic, microwaves are fundamental for the accurate determination of the resonator size and hence to relate the measured acoustic resonances with the speed of sound. As an example, in [57] measurements of the resonance frequency with accuracy of about 100 ppb permitted to obtain the mean radius of a copper-walled QSR with an extraordinary relative standard uncertainty of 0.2 ppm, which corresponded, for the employed resonator, to only 12 nm, allowing for the determination of the Boltzman constant with a relative uncertainty as low as 0.7 ppm. The potentialities of microwave resonances for length measurement is even more impressive if we consider resolution rather than accuracy: as an example, in [62] it has been shown that, even resorting to low-cost instruments, resonance changes as low as few parts per billion can be detected in copper QSRs, permitting to detect radius changes even lower than a single atomic layer.

With the new SI and the exact value of the Boltzmann coming into force, the QSRs has not been retired; conversely, in the same context, microwave resonances are now becoming fundamental for the realization and dissemination of the kelvin unit, which is now defined according to (14) as the change of thermodynamic temperature corresponding to an exact change of the thermal energy, $k_B T$ of 1.380649×10^{-23} J. The mise en pratique of the kelvin [21] identifies the AGT as one of the possible methods for its realization in the SI, with potential relative accuracy in the order of 10 ppm [10].

Along with AGT, polarizing gas thermometry (PGT), where the the thermodynamic temperature is obtained from either the dielectric constant of the gas (DCGT [17]) or its refractive index (RIGT [63]), also gained great interest in the metrological community. In particular, RIGT also relies in the measurement of microwave resonances within a QSR. While AGT uses the acoustic resonances of gas-filled QSRs to determine the speed of sound, RIGT uses microwave resonances to determine the speed of light in the same gas. From the gas refractive index n, the gas density is gathered. Then, through the equation of state of the gas and the measurement of the gas pressure p, the thermodynamic temperature T is determined. In RIGT experiments, dilute gas are exploited together with microwave frequencies, typically below 14 GHz, at which static polarizability of the gas is allowed. This simplifies the relationship between n, p and T, in the form of the Lorentz-Lorenz equation:

$$\frac{n^2 - 1}{n^2 + 2} = \frac{(A_\varepsilon + A_\mu)p}{N_A k_B T} \tag{15}$$

where A_ε and A_μ are the molar electric and magnetic polarizabilities of the gas in the limit of zero density. However, for accurate measurements, higher-order gas non-idealities must be included in the model [63]. Absolute primary RIGT using QSRs achieved relative standard uncertainties better than 35 ppm (below 10 ppm at the triple point of neon) [18].

Besides thermometry applications, the use of QSRs also permits extremely accurate measurement of the dielectric constant of pure gases or mixtures, enabling the realization of robust hygrometers and humidity standards, over extended temperature and pressure ranges [9], [12]. In [49], the skin conductivity of the copper and its thermal expansion were accurately evaluated from the resonance bandwidth, exploiting the fact that in a real metal, finite conductivity allows some current penetration into the walls at microwave frequencies.

Finally, in [13] the permittivity of helium could be determined with relative uncertainty of 100 ppb by adopting an ad-hoc developed portable and low-cost instrument, which allow to measure QSR resonances with accuracy of few tens of ppb. The adopted QSR (6 cm radius) and the instrument (KS_{21}-meter) are shown in Fig. 11. The use of field-portable low-cost instrumentation, instead of bulky laboratory one, extends the application of QSRs to the industrial field, as an example, for the measurement of humidity in methane and natural gas [64].

(a) QSR.

(b) Read-out systems: laboratory VNA vs. developed low-cost KS_{21}-meter.

FIGURE 11. Set-up for the experiment in [13].

B. WHISPERING GALLERY MODE THERMOMETRY

To perform calibrations with a high degree of accuracy, industry, commerce and scientific research would require access to a primary or secondary reference standard, i.e. an accurate, precise, stable and high-resolution system featuring a well-defined relationship between a measurable quantity and the unit of measurement of the physical quantity of interest. Since such standards are unpractical to be adopted, what it is done in practice is to adopt transfer standards, i.e. systems that are able to transfer a measurement parameter maintaining measurement traceability up to the primary standard of interest. Even if the accuracy of the transfer process can be much better than the accuracy of the transfer standard itself, the latter is required to be below few parts in 10^{-8}. Moreover, the standard must provide high resolution, stability and repeatability.

Currently, the standard platinum resistance thermometer (SPRT) is the reference transfer standard in the -196 °C to 500 °C range, for applications where measurement uncertainties below 10 mK are required. As first proposed in [48] and then demonstrated in [19], whispering-gallery-mode thermometers (WGMTs) are excellent candidates for replacing SPRTs in the -40 °C to 85 °C range, overcoming typical SPRT handling issues in a wide range of applications and providing potentially higher sensitivity. Nonetheless, the applicability of WGMTs was limited by the read-out system in charge of the resonance measurement, composed of bulky and expensive laboratory instrument. In [11] a compact but accurate WGMT is reported. The sensing element is the sapphire loaded cavity designed in [65] and shown in Fig. 12(a): a 12 mm-diameter spherical sapphire WGMR suspended in a 24 mm-cylindrical copper cavity with the highest-temperature-sensitivity mode at 13.6 GHz ($Q > 10^5$). The ad-hoc developed compact and low-cost instrumentation and data processing set employed, shown in Fig. 12(b) was instead presented in [58]. It is composed of the simplified VNA already adopted in [13], provided with a frequency extension module and a ppb-level accurate and stable frequency reference, based on a GPSDO. This set-up proved to be capable of maintaining the ppb-level accuracy in the final determination of the resonance frequency.

The WGMT was calibrated against a standard industrial PRT with 5 mK uncertainty, by fitting a cubic polynomial of

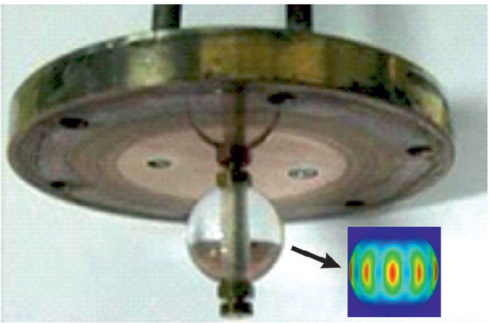

(a) WGMT sensor.

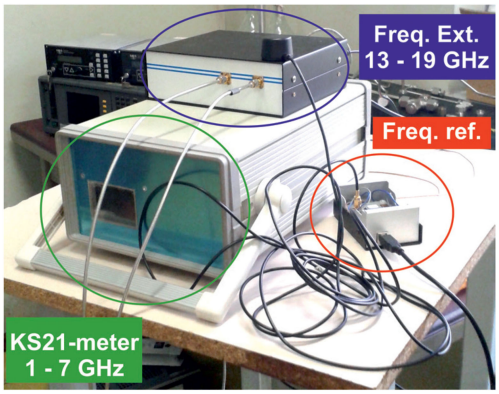

(b) WGMT read-out system.

FIGURE 12. Whispering gallery mode thermometer presented in [11].

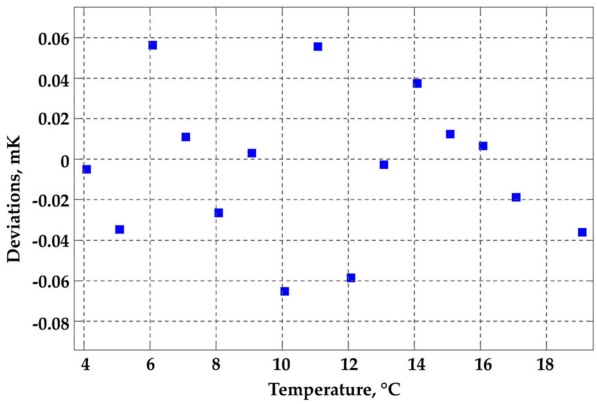

FIGURE 13. WGMT calibration fit residuals in the 4 °C to 19 °C range.

the form

$$f_0 = a_0 + a_1 T + a_2\, T^2 + a_3\, T^3 \tag{16}$$

The achieved combined standard uncertainty of 5.1 mK for a single point proved to be practically limited by this value, since the WGMT contribution was as low as 0.8 mK. In the whole −40 °C to 85 °C range large calibration residuals are recorded at specific temperature points, due to mechanical stability of the WGMR inside the cavity and by cavity sealing [43]. However, in narrow range, state-of-the-art performance, comparable with the best ITS-90 SPRTs are achieved. Calibration fit residuals within 400 μK (0 °C–20 °C), 250 μK (0 °C–20 °C) and 60 μK (4 °C–19 °C) are obtained, the latter shown in Fig. 13, demonstrating the potential use of the WGMT as an interpolating thermometer for the dissemination of the thermodynamic temperature scale.

ACKNOWLEDGMENT

The development of the low cost instrument and of the whispering gallery mode thermometer have been developed in collaboration with the Italian Institute of Metrology (INRiM).

REFERENCES

[1] W. H. Roemhild, "Using microwave sensors to measure moisture levels in mozzarella cheese," Apr. 2016. [Online]. Available: https://work-microwave.com/category/whitepaper/

[2] P. Sharma, L. Lao, and G. Falcone, "A microwave cavity resonator sensor for water-in-oil measurements," *Sens. Actuators B, Chem.*, vol. 262, pp. 200–210, Sep. 2018.

[3] W. H. Roemhild, "Microwave resonator-based sensors: An accurate solution for measuring the water content in paper," Mar. 2016. [Online]. Available: https://work-microwave.com/category/whitepaper/

[4] A. K. Jha, N. Delmonte, A. Lamecki, M. Mrozowski, and M. Bozzi, "Design of microwave-based angular displacement sensor," *IEEE Microw. Wireless Compon. Lett.*, vol. 29, no. 4, pp. 306–308, Apr. 2019.

[5] L. Essen, A. C. Gordon-Smith, and C. G. Darwin, "The velocity of propagation of electromagnetic waves derived from the resonant frequencies of a cylindrical cavity resonator," *Proc. Roy. Soc. London A., Math. Phys. Sci.*, vol. 194, no. 1038, pp. 348–361, 1948.

[6] P. Sikivie, "Experimental tests of the invisible axion," *Phys. Rev. Lett.*, vol. 51, pp. 1415–1417, Oct. 1983.

[7] R. M. Gavioso *et al.*, "Progress in INRiM experiment for the determination of the Boltzmann constant with a quasi-spherical resonator," *Int. J. Thermophys.*, vol. 32, no. 7, p. 1339, Jul. 2011.

[8] J. W. Schmidt, R. M. Gavioso, E. F. May, and M. R. Moldover, "Polarizability of helium and gas metrology," *Phys. Rev. Lett.*, vol. 98, no. 25, pp. 254504, Jun. 2007.

[9] R. Cuccaro, R. M. Gavioso, G. Benedetto, D. Madonna Ripa, V. Fernicola, and C. Guianvarc'h, "Microwave determination of water mole fraction in humid gas mixtures," *Int. J. Thermophys.*, vol. 33, no. 8-9, pp. 1352–1362, Sep. 2012.

[10] M. R. Moldover, R. M. Gavioso, J. B. Mehl, L. Pitre, M. de Podesta, and J. Zhang, "Acoustic gas thermometry," *Metrologia*, vol. 5 1, no. 1, pp. R1–R19, Jan. 2014.

[11] S. Corbellini, C. Ramella, L. Yu, M. Pirola, and V. Fernicola, "Whispering gallery mode thermometry," *Sensors*, vol. 16, no. 11, Oct. 2016, Art. no. 1814.

[12] R. J. Underwood *et al.*, "A microwave resonance dew-point hygrometer," *Meas. Sci. Technol.*, vol. 23, no. 8, pp. 085–905, Jun. 2012.

[13] S. Corbellini and R. M. Gavioso, "Low-cost instrument for the accurate measurement of resonances in microwave cavities," *IEEE Trans. Instrum. Meas.*, vol. 62, no. 5, pp. 1259–1266, Mar. 2013.

[14] G. Gennarelli, S. Romeo, M. R. Scarfi, and F. Soldovieri, "A microwave resonant sensor for concentration measurements of liquid solutions," *IEEE Sensors J.*, vol. 13, pp. 1857–1864, May 2013.

[15] M. Ikeda, A. Mase, and K. Uchino, "Measurement of dielectric parameters at microwave frequencies by cavity-perturbation technique," *Elect. Eng. Jpn.*, vol. 186, no. 2, pp. 61–67, 2014.

[16] E. F. May, L. Pitre, J. B. Mehl, M. R. Moldover, and J. W. Schmidt, "Quasi-spherical cavity resonators for metrology based on the relative dielectric permittivity of gases," *Rev. Sci. Instrum.*, vol. 75, no. 10, pp. 3307–3317, 2004.

[17] C. Gaiser, B. Fellmuth, and N. Haft, "Primary thermometry from 2.5 K to 140 K applying dielectric-constant gas thermometry," *Metrologia*, vol. 54, no. 1, pp. 141–147, Jan. 2017.

[18] P. M. C. Rourke, "NRC microwave refractive index gas thermometry implementation between 24.5 k and 84 k," *Int. J. Thermophys.*, vol. 38, no. 7, p. 107, May 2017.

[19] V. C. Fernicola and L. Yu, "Investigation of sapphire-based whispering-gallery mode resonators as transfer standard thermometers," *Meas. Sci. Technol.*, vol. 24, no. 5, p. 055106, Apr. 2013.

[20] L. Pitre *et al.*, "New measurement of the Boltzmann constant k by acoustic thermometry of helium-4 gas," *Metrologia*, vol. 54, no. 6, pp. 856–873, Jun. 2017.

[21] BIPM, "Mise en pratique for the definition of the kelvin," 2011. [Online]. Available: https://www.bipm.org/utils/en/pdf/MeP_K.pdf

[22] A. V. P. Kumar and G. Burt, "Hybrid electromagnetic modes - Structures and characteristics," in *Proc. IEEE Appl. Electromag. Conf.*, 2017, pp. 1–3.

[23] D. A. Hill, *Electromagnetic Fields in Cavities - Deterministic and Statistical Theories*, ser. IEEE Press Electromagnetic Wave Theory. Hoboken, NJ, USA: Wiley, Oct. 2009.

[24] M. R. Moldover, W. Waxman, and M. Greenspan, "Spherical acoustic resonators for temperature and thermophysical property measurements," *High Temp. High Press.*, vol. 11, pp. 75–86, 1979.

[25] J. B. Mehl, "Second-order electromagnetic eigenfrequencies of a triaxial ellipsoid," *Metrologia*, vol. 46, no. 5, pp. 554–559, Aug. 2009. [Online]. Available: https://doi.org/10.1088/0026-1394/46/5/020

[26] J. B. Mehl, "Second-order electromagnetic eigenfrequencies of a triaxial ellipsoid II," *Metrologia*, vol. 52, no. 5, pp. S227–S232, Aug. 2015.

[27] R. Underwood, D. Flack, P. Morantz, G. Sutton, P. Shore, and M. Podesta, "Dimensional characterization of a quasispherical resonator by microwave and coordinate measurement techniques," *Metrologia*, vol. 48, no. 1, Dec. 2010, Art. no. 1.

[28] M. Podesta *et al.*, "Characterization of the volume and shape of quasi-spherical resonators using coordinate measurement machines," *Metrologia*, vol. 47, no. 5, Sep. 2010, Art. no. 588.

[29] A. Parkash, J. K. Vaid, and A. Mansingh, "Measurement of dielectric parameters at microwave frequencies by cavity-perturbation technique," *IEEE Trans. Microw. Theory Techn.*, vol. 27, no. 9, pp. 791–795, Sep. 1979.

[30] D. Pozar, *Microwave Engineering*, 3rd ed. Hoboken, NJ, USA: Wiley, 2005.

[31] R. A. Waldron, "Perturbation theory of resonant cavities," *Proc. IEEE C*, vol. 107, no. 12, pp. 272–274, 1960.

[32] D. Kajfez and P. Guillon, *Dielectric Resonators (Microwave Library)*. Norwood, MA, USA: Artech House, 1998.

[33] W. E. Courtney, "Analysis and evaluation of a method of measuring the complex permittivity and permeability microwave insulators," *IEEE Trans. Microw. Theory Techn.*, vol. 18, no. 8, pp. 476–485, Aug. 1970.

[34] J. Krupka, T. Zychowicz, V. Bovtun, and S. Veljko, "Complex permittivity measurements of ferroelectrics employing composite dielectric resonator technique," *IEEE Trans. Ultrason., Ferroelectr., Freq. Control*, vol. 53, no. 10, pp. 1883–1888, 2006.

[35] J. Sheen, C.-A. Chen, Y.-H. Chen, C.-L. Lai, and Z.-W. Hong, "Microwave measurements of dielectric properties—A further study to a new theoretical model for a closed cylindrical cavity dielectric resonator," in *Proc. Eur. Conf. Antennas Propag.*, 2009, pp. 3874–3877.

[36] S. Y. Elnaggar, R. Tervo, and S. M. Mattar, "Coupled modes, frequencies, and fields of a dielectric resonator and a cavity using coupled mode theory," *J. Magn. Reson.*, vol. 238, pp. 1–7, 2014.

[37] L. Rayleigh, "CXII. The problem of the whispering gallery," *London Edinburgh Dublin Philosophical Mag. J. Sci.*, vol. 20, no. 120, pp. 1001–1004, 1910.

[38] A. E. Shitikov, I. A. Bilenko, N. M. Kondratiev, V. E. Lobanov, A. Markosyan, and M. L. Gorodetsky, "Billion Q-factor in silicon WGM resonators," *Optica*, vol. 5, no. 12, pp. 1525–1528, Dec. 2018.

[39] M. R. Foreman, J. D. Swaim, and F. Vollmer, "Whispering gallery mode sensors," *Adv. Opt. Photon.*, vol. 7, no. 2, pp. 168–240, Jun. 2015.

[40] E. N. Shaforost, N. Klein, S. A. Vitusevich, A. Offenhäusser, and A. A. Barannik, "Nanoliter liquid characterization by open whispering-gallery mode dielectric resonators at millimeter wave frequencies," *J. App. Phys.*, vol. 104, no. 7, pp. 74–111, 2008.

[41] A. Barannik, N. Cherpak, A. Kirichenko, Y. Prokopenko, S. Vitusevich, and V. Yakovenko, "Whispering gallery mode resonators in microwave physics and technologies," *Int. J. Microw. Wireless Technol.*, vol. 9, no. 4, pp. 781–796, 2017.

[42] P.-Y. Bourgeois and V. Giordano, "Simple model for the mode-splitting effect in whispering-gallery-mode resonators," *IEEE Trans. Microw. Theory Techn.*, vol. 53, no. 10, pp. 3185–3190, 2005.

[43] C. Ramella, S. Corbellini, M. Pirola, L. Yu, and V. C. Fernicola, "Investigations on instability effects in a sapphire-based whispering gallery mode thermometer," in *Proc. IEEE Int. Instrum. Meas. Technol. Conf.*, May 2017, pp. 1–6.

[44] M. Pirola, V. Teppati, and V. Camarchia, "Microwave measurements part I: Linear measurements," *IEEE Instrum. Meas. Mag.*, vol. 10, no. 2, pp. 14–19, Apr. 2007.

[45] K. Kurokawa, "The expansions of electromagnetic fields in cavities," *IRE Trans. Microw. Theory Techn.*, vol. 6, no. 2, pp. 178–187, Apr. 1958.

[46] R. Collin, *Field Theory of Guided Waves (IEEE/OUP Electromagnetic Wave Theory)*. Piscataway, NJ, USA: IEEE Press, 1990.

[47] W. G. Farr, M. Goryachev, D. L. Creedon, and M. E. Tobar, "Strong coupling between whispering gallery modes and chromium ions in ruby," *Phys. Rev. B*, vol. 90, Aug. 2014, Art. no. 054409.

[48] G. F. Strouse, "Sapphire whispering gallery thermometer," *Int. J. Thermophys.*, vol. 28, pp. 1812–18 216, Oct. 2007.

[49] P. M. C. Rourke, "NRC microwave refractive index gas thermometry implementation between 24.5 k and 84 k," *Int. J. Thermophys.*, vol. 38, no. 7, May 2017, Art. no. 107.

[50] D. Psychogiou, R. Gómez-García, R. Loeches-Sánchez, and D. Peroulis, "Hybrid acoustic-wave-lumped-element resonators (AWLRs) for high-Q bandpass filters with quasi-elliptic frequency response," *IEEE Tran. Microw. Theory Techn.*, vol. 63, no. 7, pp. 2233–2244, 2015.

[51] R. J. Underwood, J. B. Mehl, L. Pitre, G. Edwards, G. Sutton, and M. de Podesta, "Waveguide effects on quasispherical microwave cavity resonators," *Meas. Sci. Technol.*, vol. 21, no. 7, May 2010, Art. no. 075103.

[52] S. Corbellini, "A low-cost instrument for the measurement of microwave resonances in quasi-spherical cavities," in *Proc. IEEE Int. Instrum. Meas. Technol. Conf.*, 2012, pp. 641–646.

[53] S. Corbellini, C. Ramella, M. Pirola, and V. Fernicola, "A low-cost instrument for the accurate measurement of whispering-gallery resonances up to 19 GHz," in *Proc. IEEE Int. Instrum. Meas. Technol. Conf.*, May 2015, pp. 887–892.

[54] L. L. Lewis, "An introduction to frequency standards," *Proc. IEEE*, vol. 79, no. 7, pp. 927–935, Jul. 1991.

[55] J. B. Mehl, "Analysis of resonance standing-wave measurements," *J. Acoust. Soc. Amer.*, vol. 64, no. 5, pp. 1523–1525, 1978.

[56] M. Moldover, S. Boyes, C. W. Meyer, and A. Goodwin, "Thermodynamic temperatures of the triple points of mercury and gallium and in the interval 217 k to 303 k," *J. Res. Nat. Inst. Standards Technol.*, vol. 104, pp. 11–46, Apr. 1999.

[57] M. de Podesta *et al.*, "A low-uncertainty measurement of the Boltzmann constant," *Metrologia*, vol. 50, no. 4, pp. 354–376, Jul. 2013.

[58] S. Corbellini, C. Ramella, M. Pirola, V. C. Fernicola, and A. Cappella, "Low-cost instrument for whispering gallery mode thermometry up to 19 GHz," *IEEE Trans. Instrum. Meas.*, vol. 65, no. 5, pp. 1206–1214, May 2016.

[59] J. Baker-Jarvis, M. D. Janezic, and D. C. Degroot, "High-frequency dielectric measurements," *IEEE Instrum. Meas. Mag.*, vol. 13, no. 2, pp. 24–31, Apr. 2010.

[60] J. Fischer *et al.*, "Present estimates of the differences between thermodynamic temperatures and the ITS-90," *Int. J. Thermophys.*, vol. 32, pp. 12–25, Jan. 2011.

[61] J. B. Mehl and M. R. Moldover, "Measurement of the ratio of the speed of sound to the speed of light," *Phys. Rev. A*, vol. 34, pp. 3341–3344, Oct. 1986.

[62] I. Yang, R. J. Underwood, and M. Podesta, "Investigating the adequacy of a low-cost vector network analyser for microwave measurements in quasispherical resonators," *Meas. Sci. Technol.*, vol. 29, no. 7, May 2018, Art. no. 075013.

[63] P. M. C. Rourke *et al.*, "Refractive-index gas thermometry," *Metrologia*, vol. 56, no. 3, Apr. 2019, Art. no. 032001.

[64] R. Gavioso *et al.*, "Measuring humidity in methane and natural gas with a microwave technique," *Int. J. Thermophys.*, vol. 35, pp. 748–766, Mar. 2014.

[65] L. Yu and V. C. Fernicola, "Spherical-sapphire-based whispering gallery mode resonator thermometer," *Rev. Sci. Instrum.*, vol. 83, no. 9, Sep. 2012, Art. no. 094903.

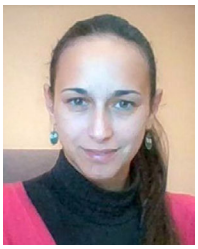

CHIARA RAMELLA (Member, IEEE) was born in Biella, Italy, in 1985. She received the M.S. degree in electronic engineering and the Ph.D. degree in electronic devices from Politecnico di Torino, Turin, Italy, in 2009 and 2013, respectively.

In 2011, she was a visiting Ph.D. student, working on cryogenic low-noise amplifiers, with Universidad de Cantabria, Santander, Spain. From 2013 to 2018, she was a Research Assistant with the Department of Electronics and Telecommunications (DET), Politecnico di Torino, Turin, Italy and from 2015 to 2016, with the Department of Electronic Engineering of Università di Roma Tor Vergata, Rome, Italy. She is currently an Assistant Professor with DET, Politecnico di Torino. Her research interests include different fields of electronics and microwave electronics, such as photocurrent amplifiers, sensor acquisition systems, microwave measurements and MMIC power amplifier design, which is her main current research interest.

MARCO PIROLA (Senior Member, IEEE) was born in Velezzo Lomellina, Italy, in 1963. He received the Laurea and Ph.D. degrees in electronic engineering from Politecnico di Torino, Turin, Italy, in 1987 and 1992, respectively.

In 1992 and 1994, he was a Visiting Researcher with Hewlett Packard Microwave Technology Division, Santa Rosa, CA, USA. From 1992 to 2000, he was a Researcher; from 2000 to 2020, he was an Associate Professor; and is currently a Full Professor with the Department of Electronics and Communications, Politecnico di Torino. His research interests include the simulation, modeling, design, and measurements of microwave devices and systems.

SIMONE CORBELLINI was born in Italy, in 1977. He received the M.S. degree in electronic engineering and the Ph.D. degree in metrology from Politecnico di Torino, Turin, Italy, in 2002 and 2006, respectively.

He is currently an Assistant Professor with Politecnico di Torino. He is involved in the development of measuring systems for the accurate measurement of resonances in microwave resonators. His current research interests include digital signal processing, distributed measurement systems, and intelligent microcontroller-based instrumentation.